Multi-physics and multi-scale deterioration modelling of reinforced concrete part I: Coupling transport and corrosion at the material scale

Michel, Alexander; Geiker, Mette Rica; Stang, Henrik; Lepech, Michael

Published in:
Proceedings of fib Symposium 2015

Publication date:
2015

Document Version
Peer reviewed version

MULTI-PHYSICS AND MULTI-SCALE DETERIORATION MODELLING OF REINFORCED CONCRETE PART I: COUPLING TRANSPORT AND CORROSION AT THE MATERIAL SCALE

Alexander Michel[1], Mette R. Geiker[2], Henrik Stang[1] and Michael Lepech[3]

[1]Technical University of Denmark, Kgs. Lyngby, DK-2800, Denmark
[2]Norwegian University of Science and Technology, Trondheim, NO-7491, Norway
[3]Stanford University, Stanford, California, 94305, USA

Abstract

In this paper, a cross disciplinary modelling framework is presented that combines physical, chemical, electrochemical, and fracture mechanical processes on different length and time scales in reinforced concrete. The theoretical background and application of finite element method (FEM) based models are sketched to describe (i) transport of heat and matter in porous media as well as phase assemblage in hardened Portland cement, (ii) corrosion of reinforcement, and (iii) material performance including corrosion-induced damages on the meso and macro scale. The presented modelling framework is fully coupled, i.e. information, such as temperature and moisture distribution, phase assemblage, corrosion current density, damage state of concrete cover, etc., are continuously exchanged between the models. Although not explicitly outlined in this paper, such an analysis may be further integrated within structural performance modelling and a full life cycle assessment to support comprehensive decision-making in order to minimize environmental, social, and economic impacts associated with the decades-long service life of reinforced concrete elements and structures.

Keywords: Service life modelling, concrete deterioration, multi-scale, multi-physics

1 Introduction

Deterioration of civil infrastructure (bridges, tunnels, roads, and buildings) together with increasing loads (e.g. traffic load and intensity) present major challenges to society in most developed countries. A major part of the infrastructure is built from concrete and costs for maintenance, renovation, and renewing are growing and by now taking up a major part of infrastructure investments. While engineering tools and methods are well developed for the structural design of new structures, tools for assessing current and predicting the future condition of reinforced concrete structures are less advanced. Existing prediction tools are largely empirical, and thus limited in their ability to predict the performance of new materials, structural, or maintenance solutions. As such, the inability to reliably assess the long-term future ramifications of today's design decisions poses a major obstacle for the design of reinforced concrete structures. A primary reason for the lack of reliable modelling tools is that deterioration mechanisms are highly complex, involve numerous coupled phenomena that must be evaluated across a range of scales, and often cut across several academic disciplines.

In this paper, a cross disciplinary modelling framework is outlined that combines physical, chemical, electrochemical, and fracture mechanical processes on different time and length scales in reinforced concrete. The theoretical background and application of finite element method (FEM) based models are sketched in this paper to describe (i) transport of heat and matter and chemical processes resulting in changes in phase assemblage in hydrated Portland cement, (ii) electrochemical processes at the reinforcement surface, and (iii) material performance including corrosion-induced damages on the meso and macro scale. Fully coupled transport of heat, matter, and ions as well as thermodynamic principles for phase changes in hydrated Portland cement are outlined in a transport and chemical module. The introduced deterioration module is based on stringent physical laws

describing thermodynamics and kinetics of electrochemical processes including various reinforcement corrosion phenomena, such as activation, resistance, and concentration polarisation as well as the impact of temperature, relative humidity, and oxygen. Corrosion-induced damages are described in a mechanical performance module, which utilizes a thermal analogy to model the expansive nature of solid corrosion products. The mechanical performance model, furthermore, accounts for the penetration of solid corrosion products into the available pore space of the surrounding cementitious material as well as non-uniform distribution of corrosion products along the circumference of the reinforcement. The modelling framework presented is fully coupled, i.e. information, such as phase assemblage, moisture distribution, corrosion rate, damage state of concrete cover, etc., are constantly exchanged between the modules.

2 Multi-physics and multi-scale modelling approach

To enable realistic and reliable long-term performance predictions as well as assessment of reinforced concrete structures, a multi-physics and multi-scale modelling framework is outlined, which is based on fundamental, science-based performance models describing various deterioration phenomena on different length scales. The basic concept of the multi-physics and multi-scale modelling framework is presented in Fig. 1. Fundamental, science-based models employed in the modelling framework deal with transport phenomena (moisture, temperature, oxygen, etc.) and phase changes in cementitious materials, electrochemistry (reinforcement corrosion), and fracture mechanics on various length and time scales. These individual science-based models, describing actual physical phenomena, are organized in groups, so-called modules in the modelling framework. To establish a link between the individual modules an interface module is required that allows for passing of information from one module to another, thereby bridging various length and time scales and allowing for concurrent performance simulations of reinforced concrete structures. The interface module may thereby be based on information-passing multi-scale (IPM) methods, thermodynamically constrained internal state variables (ISV), or local enrichment based concurrent multi-scale (LECM) methods to bridge time and length scales of the individual models describing actual deterioration phenomena in reinforced concrete. Ultimately, the interface module may be built in a standardized manner to allow for future extensions, e.g. inclusion of additional deterioration mechanisms such as freeze thaw, alkali silica reaction, of the outlined multi-physics and multi-scale modelling framework. Integration of a standardized interface module within the modelling framework will furthermore allow for adaptation of level of detailing relevant for individual cases as well as enable continuously updating based on new knowledge and to identify further research needs. In the following sections of this paper, the theoretical background of the individual modules, i.e. the full coupling of physical and chemical processes, mechanical performance, and electrochemical processes on the material scale, of the modelling framework is outlined, see Fig. 2. Results of such coupled transport, chemical, and electrochemical processes may be further used for the evaluation of structural performance as well as sustainability of reinforced concrete structures.

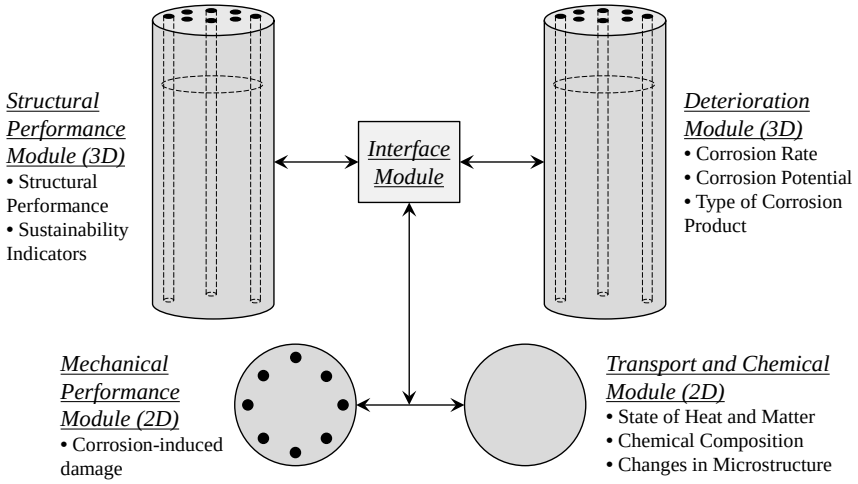

Fig. 1 Basic concept of the proposed multi-physical and multi-scale modelling framework.

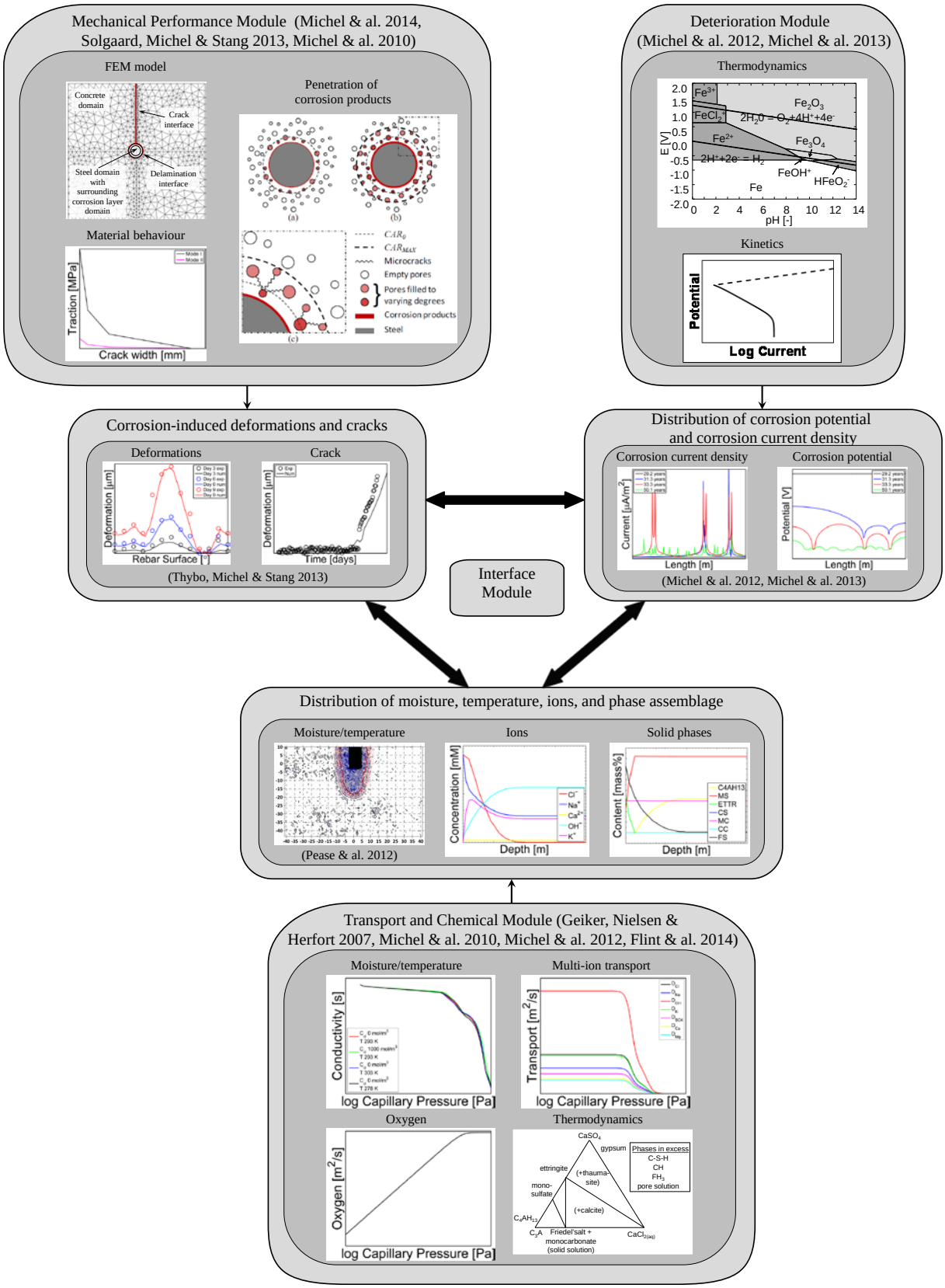

Fig. 2 Relation between mechanical performance, deterioration, and transport and chemical module within the multi-physics and multi-scale to assess deterioration in reinforced concrete structures.

3 Modelling heat, moisture, and ion transport

3.1 Coupled heat and moisture transport in porous media

Coupled heat and moisture transport in porous media, such as concrete, may be described by Richard's equation (see e.g., (Philip & de Vries 1957, Dullien 1979, Bear & Bachmat 1991)), assuming that contributions due to air transfer, gravity, radiation, liquid transport due to temperature gradients, and effects of the gaseous phase on the moisture and heat storage are negligible as well as temperatures remain below the boiling temperature of water (Janssen, Blocken & Carmeliet 2007)

$$\begin{aligned} \rho C \frac{\partial T}{\partial t} &= \nabla\left(k_{T,T}\nabla T + k_{T,pC}\nabla pC\right) \\ \frac{\partial \theta_l}{\partial p_c}\frac{\partial p_c}{\partial pC} = C_{pC}\frac{\partial pC}{\partial t} &= \nabla\left(k_{pC,pC}\nabla pC + k_{pC,T}\nabla T\right) \end{aligned} \tag{1}$$

where ρ is the mass density of concrete, C the specific heat capacity of concrete, T the temperature, t the time, pC the logarithm of the capillary pressure, θ_l the moisture content, p_c the capillary pressure, C_{pC} the moisture capacity and k transport coefficients for the heat, T, and moisture transfer, pC, respectively.

For the solution of the coupled partial differential equations (Eq. 1), material specific information on the various transport coefficients (k), capillary pressure curve (θ_{pc}) describing the moisture storage, and boundary conditions are needed. The various transport coefficients of Eq. 1 may be described as follows

$$\begin{aligned} k_{T,T} &= \lambda \\ k_{T,pC} &= -l_{lv}\frac{D_v(\Theta_l)}{R_v T}\frac{p_{v,sat}\varphi}{\rho_l R_v T}\frac{\partial p_c}{\partial pC} \\ k_{pC,pC} &= -K_l(\Theta_l)\frac{\partial p_c}{\partial pC} - \frac{D_v(\Theta_l)}{R_v T}\frac{p_{v,sat}\varphi}{\rho_l R_v T}\frac{\partial p_c}{\partial pC} \\ k_{pC,T} &= \frac{D_v(\Theta_l)}{R_v T}\frac{p_{v,sat}\varphi}{\rho_l R_v T}\frac{\partial p_{v,sat}}{\partial T} \end{aligned} \tag{2}$$

where λ is the thermal conductivity, l_{lv} the specific latent heat of evaporation, $D_v(\theta_l)$ the moisture dependent vapour diffusion coefficient, R_v the gas constant of water vapour, $p_{v,sat}$ the saturation vapour pressure, ρ_l the density of water, φ the relative humidity and $K_l(\theta_l)$ the liquid conductivity coefficient.

The moisture dependent vapour diffusion coefficient, $D_v(\theta_l)$, and the liquid conductivity coefficient, $K_l(\theta_l)$, may be described through a mechanistic modelling approach, see e.g., (Scheffler 2009, Scheffler & Plagge 2010). This mechanistic modelling approach considers thereby the microstructure of the porous media. A more thorough description of the mechanistic modelling approach can be found in Scheffler (2009) and Scheffler & Plagge (2010). To describe the moisture storage behaviour of porous media, a bimodal function of van Genuchten type may be used, see e.g., (Carmeliet & Roels 2002), which can be given as follows

$$\Theta_{p_c} = \Theta_{cap}\sum_{i=1}^{k}\frac{l_i}{(1+(a_i p_c)^{n_i})^{m_i}} \tag{3}$$

where θ_{cap} is the capillary moisture content, a_i, n_i, and m_i are shape parameters and l_i a weighting factor.

3.2 Multi-ion transport in porous media

The transport of ions in porous media is mainly governed by three different transport phenomena, i.e. diffusion, migration, and convection. Nernst-Planck equation allows for the description of multi-ion transport in porous media taking into account these transport phenomena and may be given as follows

$$\frac{\partial c_i}{\partial t} = \nabla\left(D_i \nabla c_i + z_i u_{m,i} F c_i \nabla \mathrm{E} - c_i v\right) \tag{4}$$

where the left hand term of the equation describes the change of concentration of ions considered over time, i.e. the total flux of ions. While the first term on the right hand side accounts for the diffusion of the considered ions, the second and third term describe the movement of ions due to migration, i.e. under the influence of electrostatic potentials, and convection, respectively. In the equation, c_i is the ionic concentration, D_i the ionic diffusion coefficient, z_i the charge number of the ionic species, $u_{m,i}$ the ionic mobility, F Faraday's constant, E the electrostatic potential and v the velocity of the solvent. To account for the impact of moisture on the diffusion of ions the relation proposed in Buchwald (2000) may be used

$$D_i(S_l) = D_i^0 S_l^{\xi} \tag{5}$$

where D_i^0 is the free ionic diffusion coefficient in bulk water, S_l the degree of saturation and ξ a model parameter. Binding of ions, in particular chloride binding in hardened Portland cement paste is dealt with in the next section (3.3) of this paper.

3.3 Phase assemblage in hydrated Portland cement

Ions are known to be physically adsorbed and/or chemically bound in porous media, such as concrete, commonly referred to as binding. The bound ions will not participate further in the ingress. With respect to reinforcement corrosion, especially the binding process of chloride ions is of interest as only free chloride ions may initiate reinforcement corrosion. While physical adsorption takes place at pore walls, see e.g., (Nilsson & al. 1996, Xi & Bazant 1999), mainly Friedel's salt is formed with solid cement hydration products during chemical binding, see e.g., (Nilsson & al. 1996, Birnin-Yauri & Glasser 1998, Xi & Bazant 1999). Chloride binding processes may be described by means of binding isotherms, see e.g., (Luping et al. 1993, Justnes 1998) through an apparent diffusion coefficient for chloride ions, see e.g., (Saetta, Scotta & Vitaliani 1993, Caré 2008, Bastidas-Arteaga & al. 2011).

Chloride binding in hydrated Portland cement may also be described through a thermodynamic model for the phase equilibria based on the application of the phase rule as proposed in Nielsen (2004) and Geiker, Nielsen & Herfort (2007). Calculations assume thermodynamically stable or metastable equilibrium at constant temperature and pressure, and therefore strict observance with the phase rule. The overall reaction scheme for chloride binding in hydrated Portland cement considering the total content of alkalis is given by Eq. 6 to 10, after Nielsen (2004) and Geiker, Nielsen & Herfort (2007).

Chloride binding in Portland cement pastes in which Na is still present in the C-S-H and no AFm (alumina, ferric oxide, monosulfate) phases other than monocarbonate are present may be described as follows

$$\begin{aligned} &b \cdot [C_3A \cdot CaCO_3 \cdot 11H_2O]_{(s)} + a \cdot [1.75CaO \cdot SiO_2 \cdot \omega NaOH \cdot 4H_2O]_{(s)} + \\ &\left((\kappa+1) \cdot y \cdot a + b \cdot x\right) CaCl_{2(aq)} + 2 \cdot 0.83 \cdot \kappa \cdot y \cdot aNaOH_{(aq)} \rightarrow \\ &2 \cdot \kappa \cdot y \cdot aNaCl_{(aq)} + a[1.75CaO \cdot SiO_2 \cdot (\omega - 0.34 \cdot \kappa \cdot y)NaOH \cdot yCaCl_2 \cdot 4H_2O]_{(s)} + \\ &\kappa \cdot y \cdot aCa(OH)_{2(s)} + b\left[C_3A \cdot CaCl_{2(x)} \cdot CaCO_{3(1-x)} \cdot 11H_2O\right]_{(s)} + b \cdot x\, CaCO_{3(s)} \end{aligned} \tag{6}$$

Chloride binding in Portland cement pastes in which Na is still present in the C-S-H and other AFm phases than monocarbonate are present may be described as follows

$$
\begin{aligned}
&b \cdot [C_3A \cdot CaCO_3 \cdot 11H_2O]_{(s)} + a \cdot [1.75CaO \cdot SiO_2 \cdot \omega NaOH \cdot 4H_2O]_{(s)} + \\
&\big((\kappa+1) \cdot y \cdot a + b \cdot x\big) CaCl_{2(aq)} + 2 \cdot 0.83 \cdot \kappa \cdot y \cdot aNaOH_{(aq)} \rightarrow \\
&2 \cdot \kappa \cdot y \cdot aNaCl_{(aq)} + a[1.75CaO \cdot SiO_2 \cdot (\omega - 0.34 \cdot \kappa \cdot y) NaOH \cdot yCaCl_2 \cdot 4H_2O]_{(s)} + \\
&\kappa \cdot y \cdot aCa(OH)_{2(s)} + (b + bx) \left[C_3A \cdot CaCl_{2(x)} \cdot CaCO_{3(1-x)} \cdot 11H_2O\right]_{(s)}
\end{aligned}
\tag{7}
$$

Chloride binding in Portland cement pastes with alkali-free C-S-H may be described as follows

$$
\begin{aligned}
&b \cdot \left[C_3A \cdot CaCl_{2(m)} \cdot CaCO_{3(1-m)} \cdot 11H_2O\right]_{(s)} + (b \cdot x + y \cdot a) CaCl_{2(aq)} + \\
&a \cdot [1.75CaO \cdot SiO_2 \cdot (\omega/0.34 \cdot \kappa) CaCl_2 \cdot 4H_2O]_{(s)} \rightarrow \\
&a \cdot [(1.75 - y)CaO \cdot SiO_2 \cdot (\omega/(0.34 \cdot \kappa) + y) CaCl_2 \cdot (4 - y)H_2O]_{(s)} + y \cdot aCa(OH)_{2(s)} + \\
&b \cdot [C_3A \cdot CaCl_{2(m+x)} \cdot CaCO_{3(1-m-x)} \cdot 11H_2O]_{(s)} + b \cdot xCaCO_{3(s)}
\end{aligned}
\tag{8}
$$

where a is the content of C-S-H, b the initial content of monocarbonate, ω the molar ratio of NaOH between chloride-free C-S-H and C-S-H, m the fraction of Friedel's salt in the solid solution phase at the chloride content where all alkalis have been released to the pore solution from the C-S-H, x the fraction of Friedel's salt in the AFm solid solution phase, y the content of $CaCl_2$ in the C-S-H, the relation between y and x may be described as follows

$$
\begin{aligned}
y &= 0.0601x^2 + 0.0164x \quad \text{for white Portland cement} \\
y &= 0.0376x^2 + 0.0064x \quad \text{for gray Portland cement}
\end{aligned}
\tag{9}
$$

And κ is defined as

$$
\kappa = \omega(PS/a)\ 0.2354 \tag{10}
$$

where PS is the amount of solution in millilitre.

3.4 Influence of temperature and chloride on the transport of heat and matter in porous media

Transport of moisture due to temperature gradients, also referred to as thermo diffusion, is commonly neglected, as the contribution to the total moisture transport is insignificant, see e.g., (Janssen, Blocken & Carmeliet 2007). The effect of temperature on the moisture state, however, should not be neglected. Furthermore, the impact of ion containing solutions on the vapour pressure should be taken into account. Experimental studies on the effects of temperature and chloride ions on the moisture state can be found in e.g., (Hundt & Kantelberg 1978, Bonnet 1997, Radjy, Sellevold & Hansen 2003, Ishida, Maekawa & Kishi 2007, Koniorczyk & Wojciechowski 2009). In general, the impact of temperature and chloride ions on the moisture state of porous media may be accounted for extending the state equation of the moisture storage as follows

$$
p_c = \left(p_v - \Delta p_{v,cl}\right) - p_l - \Delta p_T = \theta_{p_c}(\theta_l, c_{cl}, T) \tag{11}
$$

where p_v is the pressure of the water vapour phase, $\Delta p_{v,cl}$ is the change in vapour pressure due the presence of chloride ions, p_l the pressure of the liquid water phase, Δp_T is the change in pressure due to temperature variations, and $\theta_{pc}(\theta_l,c_{cl},T)$ is the capillary pressure curve as a function of the moisture content, θ_l, temperature, T, and chloride concentration, c_{cl}.

Since models based on stringent theories that are capable of accounting for the impact of temperature and chloride ions on the moisture state of porous media are not available in the literature, experimental data may be initially used to describe the moisture state in porous media as a function of the moisture content, θ_l, temperature, T, and chloride concentration, c_{cl}. Selected results of experimental studies on changes in the capillary pressure due to varying concentrations of chloride ions and temperature presented in Baroghel-Bouny & Wang (2011) and Hundt & Kantelberg (1978) are illustrated in Fig. 3. With respect to varying temperature, it can be observed that as temperature is increasing, the moisture content is decreasing in the hygroscopic range. On the contrary to the impact of temperature on the moisture state, it is observed that with increasing chloride concentrations increasing degrees of saturation are obtained at lower relative humidities.

Resulting moisture storage and transport properties with respect to coupled heat, mass, and multi-ion transport are presented in Fig. 4 for selected temperatures and chloride concentrations. The plots highlight the impact of varying capillary pressure, chloride concentrations, and temperature on the moisture content, moisture capacity, and conductivity. With increasing temperature the moisture content at equilibrium is decreasing as shown in Fig. 3. As the relative conductivity is dependent on microstructure of the porous media, the shape of the moisture storage function, see (Scheffler 2009, Scheffler & Plagge 2010) and subsequently the conductivity is also affected by temperature variations as illustrated in Fig. 4 (d). Fig. 4 also illustrates the impact of chlorides on the moisture storage and transport behaviour. As mentioned earlier and presented in Fig. 3, the vapour pressure above an ion containing solution is lower than in a solution containing no ions, which affects the moisture storage behaviour as presented Fig. 4 (a) and (b) and, similar to varying temperatures, alters the moisture transport properties, as illustrated in Fig. 4 (d).

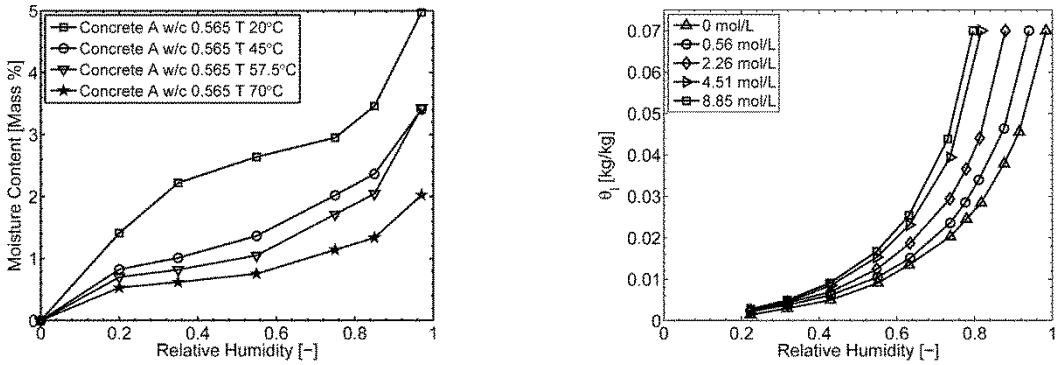

Fig. 3 Left: moisture storage for concrete at various temperatures (experimental data reproduced from Hundt & Kantelberg (1978)). Right: moisture storage of mortar specimens for varying sodium chloride concentrations (experimental data reproduced from Baroghel-Bouny & Wang (2011)).

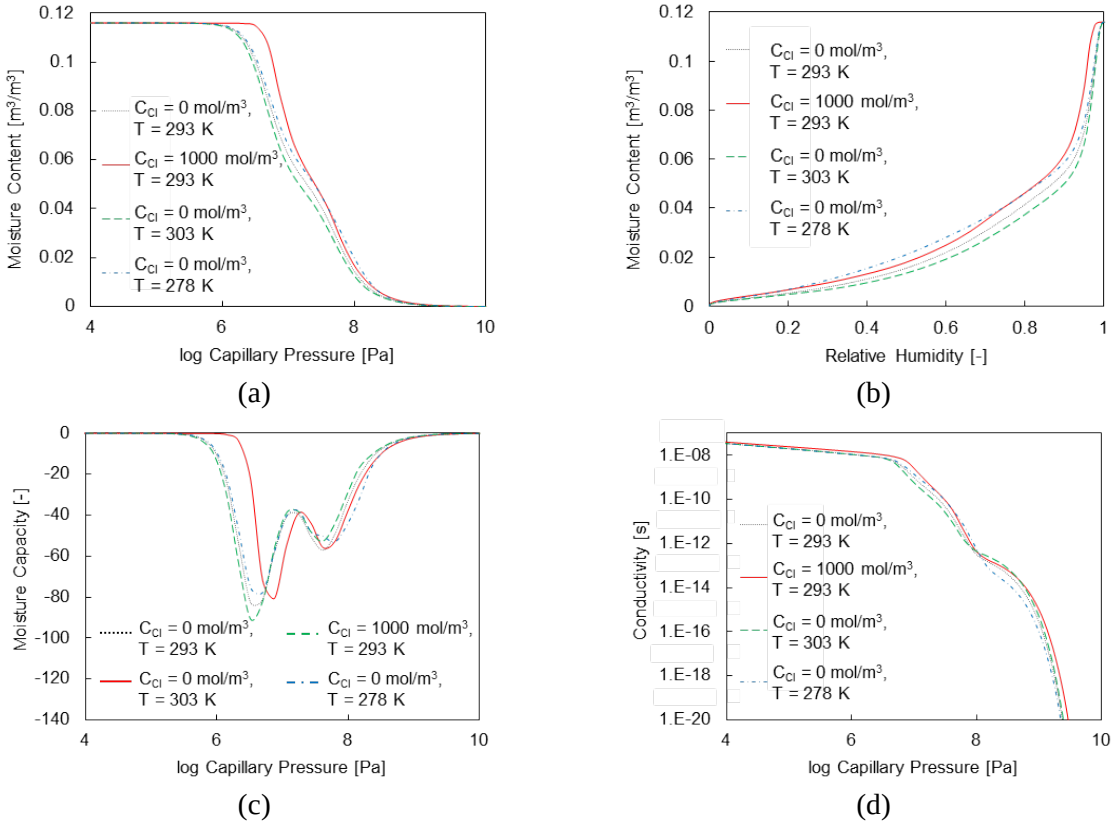

Fig. 4 (a) and (b) moisture storage behaviour, (c) moisture capacity, and (d) moisture conductivity of porous media as a function of capillary pressure and for selected temperatures and chloride concentrations (present in pore solution).

4 Modelling reinforcement corrosion

Corrosion of steel in concrete can be described by the same electrochemical processes as the corrosion of a metal in an electrolyte (Schießl 1988). An overview of fundamental electrochemical and physical processes describing the corrosion of steel in concrete is given in Fig. 5 as proposed in Küter (2009). Two electrochemical half-cell reactions must take place at the metal surface for corrosion to occur, the anodic (oxidation) and the cathodic (reduction) half-cell reaction. The anodic half-cell reaction is characterised by liberating electrons, which are consumed in the cathodic half-cell reaction. The electrons liberated at the anode are conducted through the metal to the cathode and the electrical circuit is then closed by an ionic exchange current through the concrete. Typical anodic reactions, such as the oxidation of iron are given in Eq. 12, while common cathodic reactions, such as e.g. the reduction of oxygen are presented in Eq. 13, see e.g., (Küter 2009).

$$Fe \rightarrow Fe^{2+} + 2e^{-}$$
$$2Fe + 3H_2O \rightarrow Fe_2O_3 + 6H^{+} + 6e^{-} \tag{12}$$

$$O_2 + 4H^{+} + 4e^{-} \rightarrow 2H_2O$$
$$Fe_2O_3 + 6H^{+} + 6e^{-} \rightarrow 2Fe^{2+} + 3H_2O \tag{13}$$
$$O_2 + 2H_2O + 4e^{-} \rightarrow 4OH^{-}$$

However, depending on the potential and pH at the steel surface, other cathodic reactions, such as the reduction of hydrogen or water, may take place. A detailed overview of thermodynamically feasible anodic and cathodic reactions associated with reinforcement corrosion can be found in e.g. (Küter 2009). Hence, for a thorough description of the reinforcement corrosion process, thermodynamics and kinetics must be considered.

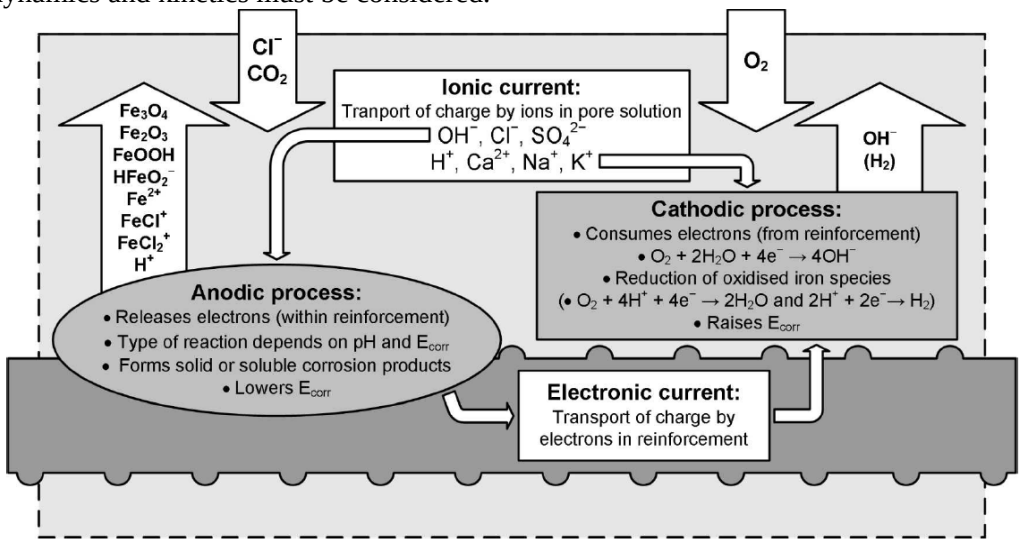

Fig. 5 Overview of electrochemical and physical processes describing corrosion of steel in concrete, from Küter (2009).

4.1 Corrosion potential and corrosion current density distribution

In principle, two physical laws may be used to describe the electrochemical processes in the concrete pore solution acting as electrolyte (Warkus, Raupach & Gulikers 2006). The first one is Laplace's equation, which describes the potential distribution in an electrolyte assuming electrical charge conservation and isotropic conductivity.

$$\nabla^2 E = 0 \tag{14}$$

The second is Ohm´s law, which may be used to determine the rate of dissolution of iron at any point on the steel surface in concrete if the potential distribution around that point and the resistivity of the electrolyte is known (Isgor & Razaqpur 2006).

$$i_{corr} = -\frac{1}{\rho_{conc}}\frac{\partial E}{\partial n} \tag{15}$$

where ρ_{conc} is the concrete resistivity and n the equipotential.

4.2 Thermodynamics of reinforcement corrosion

Among others, thermodynamics provide the possibility to investigate and assess the likelihood of reactions (in the case of reinforcement corrosion: anodic and cathodic half-cell reactions) to occur under certain conditions. To describe the equilibrium potentials, E_0, of thermodynamically feasible half-cell reactions for the corrosion process, Nernst equation can be used, which may be written as follows (Perez 2004)

$$E_0 = E_0^0 - \frac{RT}{zF} ln\left(\frac{\alpha_{Red/Ox}}{\alpha_{Ox/Red}}\right) \tag{16}$$

where E_0^0 is the standard equilibrium potential, R the gas constant, and $\alpha_{Red/Ox}$ the chemical activity of the reductant and oxidant, respectively.

Nernst equation may be further used to construct pH - potential diagrams, or more frequently called Pourbaix diagrams, providing a graphical overview of thermodynamically favoured reactions (i.e. reactions with a negative free enthalpy) as a function of the pH and the half-cell potential. The Pourbaix diagram for iron in chloride ion containing water (commonly used to investigate corrosion reactions of steel in concrete (Küter 2009)) is illustrated in Fig. 6. In combination with the information from the transport and chemical module (i.e. transport of ions and phase assemblage), the pH in the concrete pore solution can be determined. Along with the electric potential, determined from Laplace equation, thermodynamically feasible anodic and cathodic reactions can then be selected when modelling reinforcement corrosion processes. For example, in case of carbonation-induced reinforcement corrosion, a considerable pH drop is observed as a result of carbon dioxide ingress. The pH in a carbonated concrete is around 8, and the anodic half-cell potential is around -0.2 V_{SHE}. Under these conditions, thermodynamically feasible reactions are the oxidation of iron and reduction of oxygen, respectively, see Fig. 6 for comparison.

$$\begin{aligned} Fe &\rightarrow Fe^{2+} + 2e^- \\ O_2 + 4H^+ + 4e^- &\rightarrow 2H_2O \end{aligned} \tag{17}$$

In a similar fashion, thermodynamically feasible reactions depending on the pH and half-cell potential in the vicinity of the reinforcement surface can be selected and adjusted when modelling corrosion processes in case of chloride-induced reinforcement corrosion.

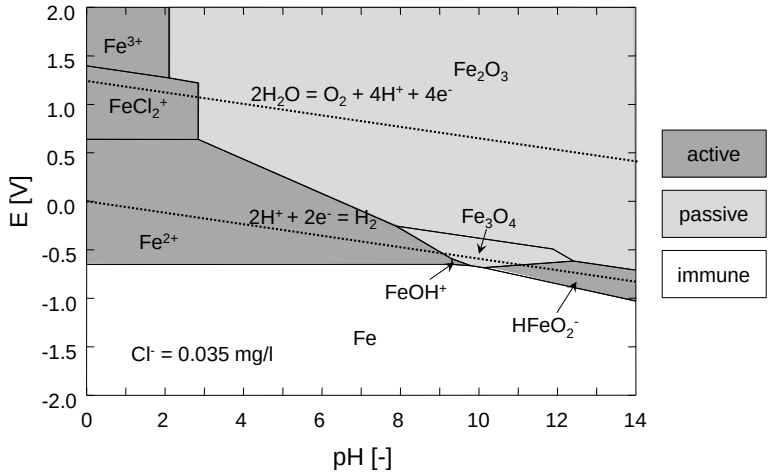

Fig. 6 Pourbaix diagram for Fe-Cl-H_2O system at 25°C, with an Fe ion activity of 10^{-6} mol/L and Cl concentration of 0.035 mg/L, after [Küter 2009].

4.3 Kinetics of reinforcement corrosion

Although thermodynamics provide means to assess the possibility of corrosion reactions to occur under various conditions, no information on the rate of these reactions is obtained. Therefore, the kinetics of electrochemical reactions must be considered to fully assess the corrosion mechanism. Once corrosion is initiated, the potentials of the half-cell reactions on the steel surface are shifted from their equilibrium potentials and a (corrosion) current will start to flow. The shift from the equilibrium potential is known as polarisation and the kinetics of the electrochemical half-cell reactions are governed by the degree of polarisation. A measure for the polarisation is the overpotential, η, which is the difference between the half-cell potential, $E_{c/a}$, and the equilibrium potential, $E_{0a/0c}$. Information on the polarisation of electrodes (anode and cathode) can be summarised in so-called Evan's diagrams relating the half-cell potential to the corrosion current. The Evan's diagram for the anodic and cathodic half-cell reactions assuming the formation of Fe^{2+} at the anode and OH^- at the cathode is given in Fig. 7. The corrosion potential (also referred to as mixed potential), E_{corr}, and the corrosion current density, i_{corr}, can be determined from the intersection of the anodic and the cathodic polarisation curve.

Depending on the mechanism, four types of polarisation acting individually or in combination may be distinguished; namely, activation, concentration, resistance, and crystallisation polarisation (Shreir 1994). With respect to reinforcement corrosion, crystallisation polarisation can be neglected and only the effects of activation, concentration, and resistance polarisation may be taken into account, sees e.g., (Fontana & Greene 1978, Bardal 2004).

For activation polarisation, the relation between the corrosion current and the half-cell potential may be described by the Butler-Volmer equation as follows (assuming that the electrochemical reactions take place at separate electrodes and the polarisation is high) (Stern & Geary 1957)

$$i = i_0 exp(\Psi) \;\; with \;\; \Psi = ln(10)\frac{E - E_0}{b_T} \tag{18}$$

where i is the corrosion current density, i_0 the exchange current density, and b_T the Tafel constant, which is defined as follows

$$b_T = ln(10)\frac{RT}{\alpha zF} \tag{19}$$

where α is the symmetry factor. To include the effects of concentration polarisation on the relation between the half-cell potential and the corrosion current density, Eq. 18 may be extended and written as follows (Böhni 2005)

$$i = i_0 exp\left(\frac{1 - \Psi}{1 + \mathrm{i_0/i_{lim}}\Psi}\right) \tag{20}$$

where i_{lim} is the limiting corrosion current density, which may be defined as follows (Bardal 2004)

$$i_{lim} = \frac{zFD_{O2}}{\delta}c_{O2} \tag{21}$$

where D_{O2} is the oxygen diffusion coefficient, c_{O2} the oxygen concentration at the electrode surface and δ the diffusion layer thickness.

A number of factors influence the shape of the polarisation curve, which in turn governs the kinetics of the corrosion process. Among others, the surface state of the electrode, temperature, moisture content, and geometry are decisive for the overpotential at the anode and cathode (Bardal 2004). For example, the temperature, moisture content, and geometry are important parameters for diffusion-controlled corrosion. A high moisture content considerably hinders the oxygen transport from the concrete surface to the electrode. This may lead to a depletion of oxygen at the cathode ceasing the cathodic half-cell reaction (assuming reduction of oxygen as governing half-cell reaction) and subsequently the corrosion process itself. Furthermore, several electrochemical parameters, such as the exchange current density or the equilibrium potential are influenced by temperature (see e.g., Eq. 16 and 19). This highlights the importance of a fully coupled modelling framework, i.e. coupling

between mass and heat transport, phase assemblage, and kinetics and thermodynamics of reinforcement corrosion, for a reliable and realistic assessment as well as long term prediction of the performance of reinforced concrete structures with respect to corrosion.

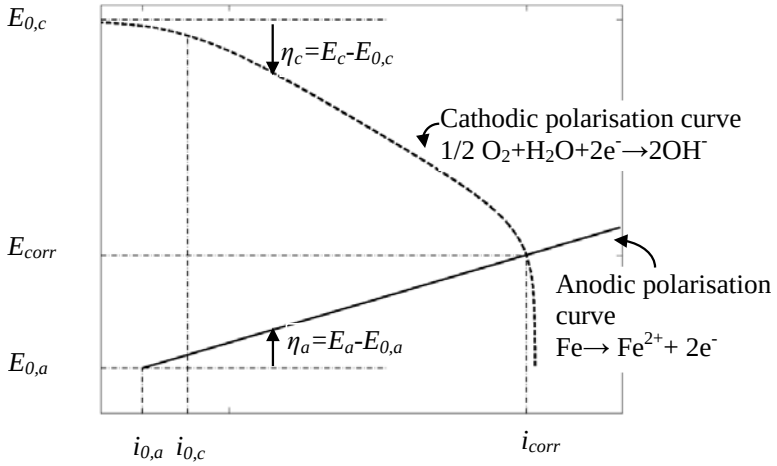

Fig. 7 Evan's diagram illustrating the anodic and cathodic polarisation on the steel surface, after (Martín-Pérez 1999).

4.4 Initiation of reinforcement corrosion

To link corrosion initiation, i.e. the formation of anodic regions at the reinforcement surface, and propagation of reinforcement corrosion a conditional statement may be defined along the reinforcement surface. In case of chloride-induced corrosion, the conditional statement may comprise the definition of a critical chloride threshold for elements along the reinforcement surface, which might be defined as follows

$$BC_{Steel} = \begin{cases} i_a \\ i_c \end{cases} for \begin{matrix} c_{cl} \geq c_{crit} \\ c_{cl} < c_{crit} \end{matrix} \tag{22}$$

where BC_{Steel} is the boundary condition along the steel surface, i_a the anodic polarisation curve (see Eq. 18), i_c the cathodic polarisation curve (see Eq. 20), c_{cl} the chloride concentration along the reinforcement, and c_{crit} the critical chloride threshold defined along the reinforcement. Within the literature, varying critical chloride threshold values can be found, ranging from 0 to approximately 2% of weight cement (Angst & al. 2009). Among others, the critical chloride threshold is influenced by defects present along the reinforcement (Buenfeld & al. 2004, Nygaard & Geiker 2005), material properties, length of reinforcement, and exposure conditions (*fib* 1992) as well as the electrochemical potential (Angst & al. 2009). As an approximation, the critical chloride threshold may be varied randomly along the reinforcement surface, ranging from 0 to 2% of weight cement, to account for the influence of various parameters and represent a realistic reinforced concrete structure with defects, voids, etc. present at the concrete steel interface. A similar conditional statement for elements along the steel surface may be derived in case of carbonation-induced corrosion.

5 Modelling corrosion-induced concrete damage

Once corrosion is initiated, electrochemical half-cell reactions are taking place along the reinforcement, see Section 4.2. The ionic reaction products of these half-cell reactions may further react and form solid corrosion products in the vicinity of the reinforcement. The type of corrosion products formed; depend on the thermodynamic conditions present in the vicinity of the reinforcement (Küter 2009). Apart from solid corrosion products, soluble iron-chloride complexes (also referred to as green rust) may form in an oxygen-deprived environment in which chlorides are present (Koleva & al. 2006, Küter 2009). Such soluble iron-chloride complexes may not necessarily form in the vicinity of the reinforcement surface, as shown e.g. in Küter (2009).

Independent of the type of iron oxides formed as a result of active corrosion, the iron oxides occupy a larger volume than the initial iron that is consumed during the corrosion reaction, see e.g.,

(Alonso & al., 1998, Marcotte & Hansson 2007). The increased volume of corrosion products causes tensile stresses in the surrounding concrete and may lead to concrete cracking, spalling, or delamination if the tensile strength of the concrete is exceeded.

5.1 Modelling approach

A thermal analogy may be used to model corrosion-induced concrete damage due to the expansive nature of solid corrosion products. Assuming uniform distribution of corrosion along the reinforcement, the model may be formulated as a 2D plain strain problem. Corrosion-induced damage may then be described through a discrete cracking approach in which the tension softening behaviour of concrete can be approximated through multi-linear softening relations, see e.g., (Skoček & Stang 2008). Basic geometrical considerations, assumed crack propagation, and methodology of load application to simulate corrosion-induced damage in reinforced concrete by means of such a thermal analogy are illustrated in Fig.8 and 9.

For the determination of the corroded reinforcement section, Faraday´s law may be used relating the thickness reduction per time unit to the corrosion current density (predicted by the deterioration module).

$$X(t) = \frac{M_{Fe}}{zF\rho_{Fe}} \int_0^t i_{corr}\,(t)dt \tag{23}$$

where $X(t)$ is the cross sectional reduction of the reinforcement as a function of time, t, M_{Fe} the molar mass of iron, and ρ_{Fe} the density of iron. Assuming a constant coefficient of thermal expansion, α, the applied temperature increment, ΔT, represents then the type of solid corrosion product (see Fig. 7). Assuming further isotropic material properties of the corrosion products, the linear expansion coefficient may be obtained as one third of the volume expansion coefficient.

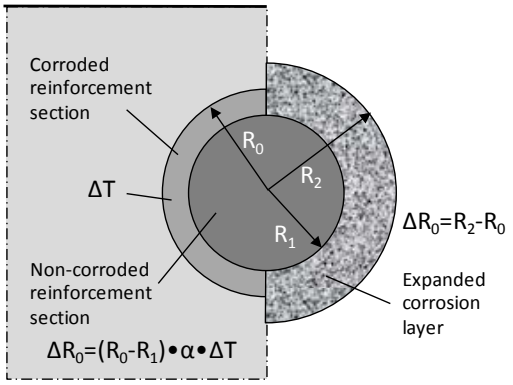

Fig. 8 Load application and geometrical considerations to simulate corrosion-induced concrete cracking, from Michel & al (2010).

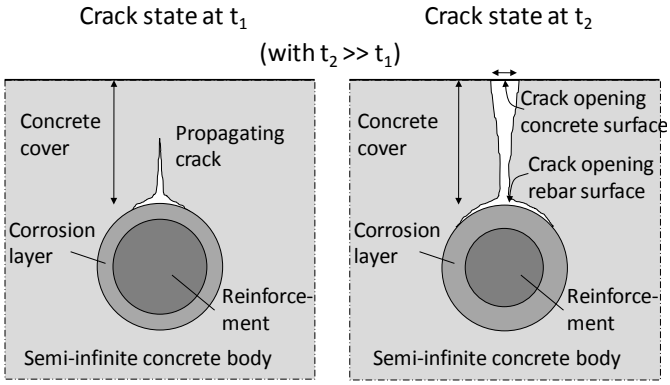

Fig. 9 Assumed crack propagation to simulate corrosion-induced concrete cover cracking, from Michel & al. (2010).

5.2 Penetration of corrosion products

The penetration of corrosion products has a major influence on the predicted time-to-crack initiation and crack propagation; see e.g., (Liu & Weyers 1998, Val, Chernin & Stewart 2009). The corrosion accommodation region, *CAR*, also referred to as "diffusion" or "porous" zone, describes a region of concrete around the reinforcement, which can accommodate expansive corrosion products delaying stress development in the concrete. The accommodation of corrosion products in the *CAR* may be accounted for by an adjusted temperature increment, ΔT_{CAR} (see Fig. 8) as follows

$$\Delta T_{CAR} = \lambda_{CAR} \Delta T \tag{24}$$

where λ_{CAR} describes the penetration of corrosion products into the accessible space of the cementitious matrix, V_{CAR}. Based on experimental observations presented in Michel & al. (2011) and Michel & al. (2014), a conceptual schematic to include the penetration of solid corrosion products in the simulation of corrosion-induced concrete damage is shown in Fig. 10. The concept assumes that an

initial corrosion accommodating region (*CAR*) around the reinforcement exists, denoted CAR_0, which delays stress formation while filling with solid corrosion products. Once this initial CAR_0 is filled with corrosion products, tensile stresses in the surrounding cementitious material will increase and potentially lead to the formation of micro-cracks. These micro-cracks allow solid corrosion products to penetrate additional pore spaces and further delay corrosion-induced stresses. At some point a maximum size of the *CAR*, denoted as CAR_{MAX}, is reached. No corrosion products can penetrate the matrix of the cementitious material beyond that point and all additionally formed corrosion products will introduce tensile stresses and potentially lead to the formation of a macro-crack. λ_{CAR} describing the penetration of corrosion products into the accessible space of the cementitious matrix may thereby be approximated as follows

$$\lambda_{CAR} = \begin{cases} \left(\frac{V_{cp}}{V_{CAR}}\right)^n & if \ V_{cp} < V_{CAR} \\ 1 & V_{cp} \geq V_{CAR} \end{cases} \tag{25}$$

where V_{cp} is the volume of corrosion products and n a non-physical fitting parameter. More detailed information on the mathematical description of the penetration of corrosion products into the accessible pore space of cementitious materials can be found in Michel & al. (2013).

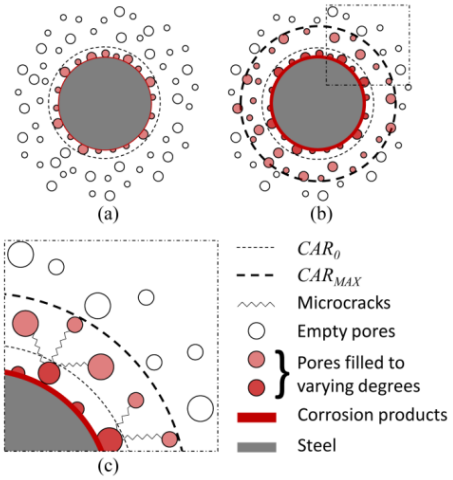

Fig. 10 Conceptual schematic to describe the penetration of solid corrosion products, where (a) shows the initial CAR_0, (b) the increase in *CAR* size to a maximum, and (c) the formation of micro-cracks between pores, from Michel & al. (2013).

6 Summary and conclusions

In this paper, the theoretical background and coupling of chemical, electrochemical, and fracture mechanical processes on different length and time scales in reinforced concrete within a novel cross disciplinary modelling framework was presented. The presented multi-physics and multi-scale model for corrosion in reinforced concrete structures deals with (i) the transport of heat and matter as well as phase assemblage in hydrated Portland cement, (ii) corrosion of reinforcement, and (iii) material performance including corrosion-induced damages on the meso and macro scale. The modelling framework presented is fully coupled, i.e. information, such as phase equilibria, moisture distribution, corrosion rate, damage state of concrete cover, etc., are constantly exchanged between the modules, see Fig. 2.

Outcomes of the fully coupled mechanical performance, deterioration, and transport and chemical modules described within this paper may be used for further analysis and coupling within a structural performance module, see Fig. 11. In particular, cross sectional reduction of reinforcement due to corrosion and concrete cover damage may be used within such a structural performance module to determine (i) structural performance of deteriorated concrete members, (ii) change in reinforcement bond strength due to formation of oxidation products, (iii) reduction in capacity of corroded reinforcing bars, (iv) reduction in ductility of corroded reinforcing bars, and (v) buckling of corroded reinforcing bars to assess the structural effects of reinforcement corrosion on concrete structures.

Additionally, such an analysis may be further integrated within a full life cycle assessment to support comprehensive decision-making in order to minimize environmental, social, and economic impacts associated with the decades-long service life of reinforced concrete elements and structures.

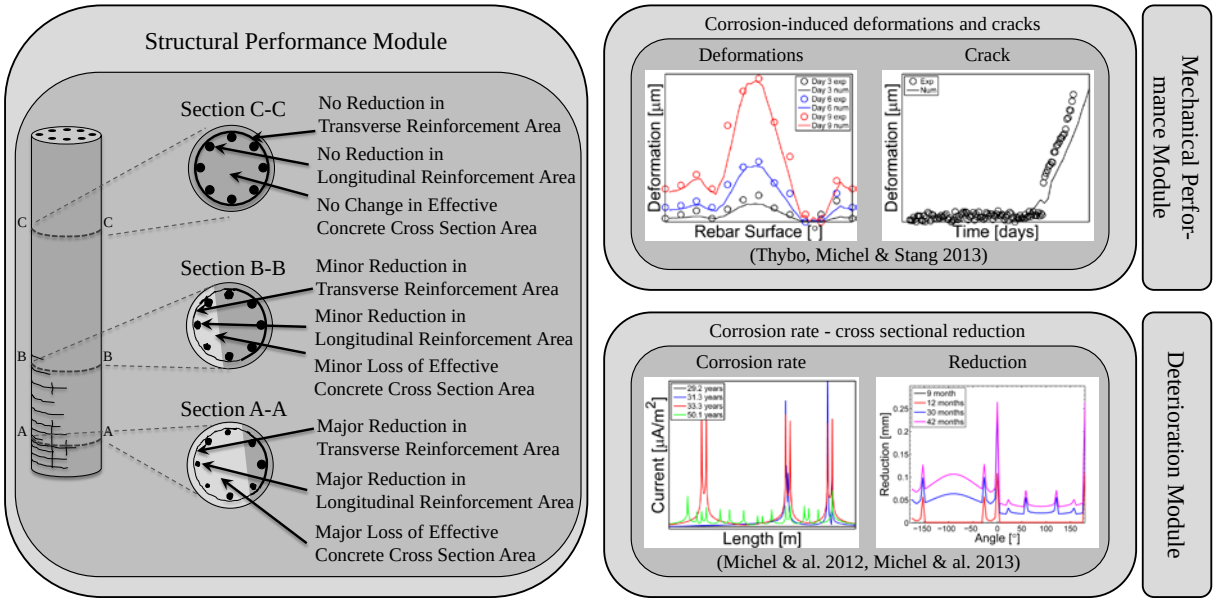

Fig. 11 Schematic representation of link between mechanical performance, deterioration, and structural performance module. Information on cross sectional area reduction of reinforcement and concrete cover damage along the length of the member are exchanged between the modules.

Acknowledgements

The first author gratefully acknowledges the financial support of Femern Bælt A/S, Sund & Belt Holding A/S and The Danish Agency for Science, Technology and Innovation. Financial contributions from the Danish Expert Centre for Infrastructure Constructions, COWIfonden, and the project 'Sustainable Rehabilitation of Civil and Building Structures' funded by Nordic Innovation Centre, Project No. 08190 SR are also greatly appreciated.

References

Alonso, C., Andrade, C., Rodriguez, J., & Diez, J.M. (1998) Factors controlling cracking of concrete affected by reinforcement corrosion, Materials and Structures, 31(211):435-441.

Angst, U., Elsener B., Larsen, C.K. & Vennesland, Ø. (2009) Critical chloride content in reinforced concrete - A review, Cement and Concrete Research, 39(12):1122-1138.

Bardal, E. (2004) Corrosion and Protection, Springer-Verlag, London, UK.

Baroghel-Bouny, V. & Wang, X. (2011) Modelling of isothermal coupled moisture-ion transport in cementitious materials, Cement and Concrete Research, 41(8):828-841.

Bastidas-Arteaga, E., Chateauneuf, A., Sánchez-Silva, M., Bressolette, P. & Schoefs, F. (2011) A comprehensive probabilistic model of chloride ingress in unsaturated concrete, Engineering Structures, 33:720-730.

Bear, J. & Bachmat, Y. (1991) Introduction to modeling of transport phenomena in porous media. Dordrecht, Kluwer Acad. Publ.

Birnin-Yauri, U. & Glasser, F. (1998) Friedel's salt, Ca2Al(OH)6(Cl,OH)•2H2O: Its solid solutions and their role in chloride binding, Cement and Concrete Research, 28(12):1713-1723.

Bonnet, S. (1997) Influence of chloride on equilibrium behaviour and on transfer properties of civil engineering materials, (in French), Ph.D. thesis, INSA, Toulouse, France.

Böhni, H. (2005) Corrosion in reinforced concrete structures, Woodhead Publishing Ltd.

Buchwald, A. (2000) Determination of the ion diffusion coefficient in moisture and salt loaded masonry materials by impedance spectroscopy, In: Proceedings of 3rd International PhD Symposium 2, Vienna.

Buenfeld, N., Glass, G., Reddy, B., & Viles, F. (2004) Process for the Protection of Reinforcement in Reinforced Concrete, United States Patent 6685822, USPTO, Alexandria, VA, USA.

Caré, S. (2008) Effect of temperature on porosity and on chloride diffusion in cement pastes, Construction and Building Materials, 22:1560-1573.

Carmeliet, J. & Roels, S. (2002) Determination of the moisture capacity of porous building materials, Journal of Building Physics, 25(3):209-237.

Dullien, F.A.L. (1979) Porous Media: Fluid Transport and Pore Structure, Academic Press.

fib Bulletin 183 (1992) Durable Concrete Structures, Technical Report *fib* Bulletin 34, International Federation for Structural Concrete (*fib*), Lausanne, Switzerland, 2nd edition. 112 pp.

Flint, M.M., Michel, A., Billington, S.L. & Geiker, M.R. (2014) Influence of Temporal Resolution of Boundary Conditions on the Moisture, Temperature and Ion Distributions in Concrete, Materials and Structures, 47(4):729-748.

Fontana, M.G. & Greene, N.D. (1978) Corrosion engineering, McGraw-Hill.

Geiker, M., Nielsen, E.P. & Herfort, D. (2007) Prediction of chloride ingress and binding in cement paste, Materials and Structures, 40:405-417.

Hundt, J. & Kantelberg, H. (1978) Sorptionsuntersuchungen an Zementstein, Zementmörtel und Beton, Deutscher Ausschuss für Stahlbeton, 297:25-39.

Isgor, B.O. & Razaqpur, G.A. (2006) Modelling steel corrosion in concrete structures, Materials and Structures, 39(287):291-302.

Ishida, T., Maekawa, K. & Kishi, T. (2007) Enhanced modeling of moisture equilibrium and transport in cementitious materials under arbitrary temperature and relative humidity history, Cement and Concrete Research, 37:565-578.

Janssen, H., Blocken, B. & Carmeliet, J. (2007) Conservative modelling of the moisture and heat transfer in building components under atmospheric excitation, International Journal of Heat and Mass Transfer, 50(5):1128-1140.

Koleva, D.A., Hu, J., Fraaij, A.L.A., Stroeven, P., Boshkov, N., & de Wit, J.H.W. (2006) Quantitative characterisation of steel/cement paste interface microstructure and corrosion phenomena in mortars suffering from chloride attack, Corrosion Science, 48(12):4001-4019.

Koniorczyk, M. & Wojciechowski M. (2009) Influence of salt on desorption isotherm and hygral state of cement mortar - Modelling using neural networks, Construction and Building Materials, 23:2988-2996.

Küter, A. (2009) Management of reinforcement corrosion: a thermodynamical approach, Ph.D. thesis, Technical University of Denmark, Kgs. Lyngby, Denmark.

Liu, Y. & Weyers, R.E. (1998) Modeling the time-to-corrosion cracking in chloride contaminated reinforced concrete structures, ACI Materials Journal, 95(5):675-681.

Marcotte, T. & Hansson, C. (2007) Corrosion products that form on steel within cement paste, Materials and Structures, 40(3):325-340.

Martín-Pérez, B. (1999) Service Life Modelling of R.C. Highway Structures Exposed to Chlorides, Ph.D. thesis, University of Toronto, Toronto, Canada.

Michel, A., Solgaard, A.O.S., Geiker, M.R., Stang, H. & Olesen, J.F. (2010) Modeling Formation of Cracks in Concrete Cover due to Reinforcement Corrosion, Proceedings of FraMCos 7 (7th International Conference on Fracture Mechanics of Concrete and Concrete Structures), May 23-28, 2010, Jeju, Korea.

Michel, A., Pease, B.J., Geiker, M.R. Stang, H. & Olesen, J.F. (2011) Monitoring reinforcement corrosion and corrosion-induced cracking using non-destructive x-ray attenuation measurements, Cement and Concrete Research, 41:1085-1094.

Michel, A. Geiker, M.R., Stang, H. & Olesen, J.F. (2012) Modelling Reinforcement Corrosion in Concrete, In: Proceedings of MicroDurability, April 11-13, 2012, Amsterdam, Netherlands.

Michel, A., Geiker, M.R., Stang, H. & Lepech, M. (2013) Integrated modelling of corrosion-induced deterioration in reinforced concrete structures, In: Proceedings of Eurocorr 2013, 1-5 September, 2013, Estoril, Portugal.

Michel, A. Pease, B.J., Peterová, A. Geiker, M.R., Stang, H. & Thybo, A.E.A. (2014) Penetration of corrosion products and corrosion-induced cracking in reinforced cementitious materials: experimental investigations and numerical simulations, Cement and Concrete Composites, 47:75-86.

Nielsen, E.P. (2004) The durability of white Portland cement to chemical attack, Ph.D. thesis, Technical University of Denmark, Kgs. Lyngby, Denmark.

Nilsson, L.O., Poulsen, E., Sandberg, P., Sørensen, H.E. & Klinghoffer, O. (1996) Hetek, chloride penetration into concrete state-of-the-art-transport processes, corrosion initiation, test methods and prediction models, Technical Report: Report No. 53, The Danish Road Directorate.

Nygaard, P.V. & Geiker, M.R. (2005) A method for measuring the chloride threshold level required to initiate reinforcement corrosion in concrete, Materials and Structures, 38:489-494.

Pease, B.J., Michel, A., Geiker, M.R. & Stang, H. (2012) Modelling Moisture Ingress through Simplified Concrete Geometries, In: Proceedings of ICDC, June 17-21, 2012, Trondheim, Norway.

Perez, N. (2004) Electrochemistry and Corrosion Science, Kluwer Academic Publishers, Boston.

Philip, J.R. & de Vries, D.A. (1957) Moisture movement in porous materials under temperature gradients, Transactions of the American Geophysical Union, 38:222-232.

Radjy, F., Sellevold, E.J. & Hansen, K.K. (2003) Isosteric vapor pressure - temperature data for water sorption in hardened cement paste: enthalpy, entropy and sorption isotherms at different temperatures, Report BYG-DTU R057, Technical University of Denmark (DTU), Kgs. Lyngby, Denmark.

Saetta, A.V., Scotta, R.V. & Vitaliani, R.V. (1993) Analysis of chloride diffusion into partially saturated concrete, ACI Materials Journal, 90(5):441-45.

Scheffler, G.A. (2009) Validation of hygrothermal material modelling under consideration of the hysteresis of moisture storage, Ph.D. thesis, Technical University of Dresden, Dresden, Germany.

Scheffler, G.A. & Plagge, R. (2010) A whole range hygric material model: Modelling liquid and vapour transport properties in porous media, International Journal of Heat and Mass Transfer, 53(1-3):286-296.

Schießl, P. (Ed.) (1988) Corrosion of steel in concrete, Report of the Technical Committee 60 CSC, RILEM, Chapman and Hall.

Shreir, L.L. (1994) Corrosion in Aqueous Solutions, In Shreir, L.L., Jarman, R.A. & Burstein, G.T. editors, Corrosion Volume 1 Metal/Environment Reactions, Butterworth-Heinemann, Boston.

Skoček, J. & Stang, H. (2008) Inverse analysis of the wedge-splitting test, Engineering Fracture Mechanics, 75:3173-3188.

Solgaard, A.O.S., Michel, A. & Stang, H. (2013) Concrete cover cracking due to uniform reinforcement corrosion, Materials and Structures, 46(11):1781-1799.

Stern, M. & Geary, A.L. (1957) Electrochemical polarization I. A theoretical analysis of the shape of polarization curves, Journal of the Electrochemical Society, 104:56-63.

Thybo, A.E.A., Michel, A. & Stang, H. Modelling of corrosion-induced concrete damage, FraMCos-8 - 8th International Conference on Fracture Mechanics of Concrete and Concrete Structures, 10-14 March, 2013, Toledo, Spain.

Val, D.V., Chernin, L. & Stewart, M.G. (2009) Experimental and numerical investigation of corrosion-induced cover cracking in reinforced concrete structures, Journal of Structural Engineering, 135(4):376-385.

Warkus, J., Raupach, M. & Gulikers, J. (2006) Numerical modeling of corrosion - Theoretical backgrounds -, Materials and Corrosion, 57: 614-617.

Xi, Y. & Bazant, Z. (1999) Modeling chloride penetration in saturated concrete, Journal of Materials in Civil Engineering, 11(1):58-65.